Materials Research Bulletin 98 (2018) 300–307

Contents lists available at ScienceDirect

Materials Research Bulletin

journal homepage: www.elsevier.com/locate/matresbu

Ultrasensitive and selective non-enzymatic electrochemical glucose sensor based on hybrid material of graphene nanosheets/graphene nanoribbons/nickel nanoparticle

L. Jothi[a], N. Jayakumar[a], S.K. Jaganathan[b,c,d], G. Nageswaran[a,*]

[a] Department of Chemistry, Indian Institute of space science and Technology, Thiruvananthapuram, Kerala, 695547, India
[b] Department for Management of Science and Technology Development, Ton Duc Thang University, Ho Chi Minh City, Vietnam
[c] Faculty of Applied Sciences, Ton Duc Thang University, Ho Chi Minh City, Vietnam
[d] IJN-UTM Cardiovascular Engineering Centre, Faculty of Biosciences and Medical Engineering, Universiti Teknologi Malaysia, Skudai 81300, Johor, Malaysia

ARTICLE INFO

Keywords:
Nickel nanoparticle
Graphene sheet
Graphene nanoribbon
Non-enzymatic glucose sensor
Amperometric

ABSTRACT

A fast, highly sensitive and selective non-enzymatic electrochemical glucose sensor based on graphene sheet/graphene nanoribbon/nickel nanoparticles (GS/GNR/Ni) hybrid material modified electrode was fabricated. The hybrid material was synthesized via facile in-situ chemical reduction and characterized by X-ray diffraction, transmission electron microscopy, Raman spectroscopy, cyclic voltammetry and electrochemical impedance spectroscopy. The GS/GNR/Ni/GCE showed high electrochemical activity towards the oxidation of glucose in a 0.1 M NaOH solution. At an applied potential of +0.5 V, it displayed wide linear amperometric response towards glucose from the range of 5 nM–5 mM, with a detection limit of 2.5 nM and sensitivity of 2.3 mA/mM cm^2. Moreover, the modified electrode was relatively insensitive to commonly interfering species such as dopamine, ascorbic acid, sucrose, uric acid and Cl^- ions. The fabricated sensor with better reproducibility, good long term stability, makes it a promising electrode for the development of effective glucose sensor.

1. Introduction

Diabetes mellitus, a chronic disease related to glucose digestion caused by insufficient insulin secretion, causes increasing death rate worldwide. Therefore determination of glucose level in blood is of practical importance to reduce the complications associated with diabetes. In recent years considerable research have been devoted in development of vast number of rapid, sensitive and accurate glucose sensors to monitor glucose which are not only relevant for determination of glucose level in blood but also in the food industry, bioprocessing, etc [1]. Among the various available analytical methods [2–5], electrochemical glucose sensor has been widely used due to its merits including high sensitivity, time efficiency, simplicity, excellent selectivity, rapid response, lowest detection limit and good reliability [6]. Since the development of the first ever enzymatic glucose sensor by Clark and Lyons in 1962 [7], the enzymatic glucose sensor based on glucose oxidase (GOD) developed for self-testing and continuous glucose monitoring dominates the biosensor industry. However, the intrinsic flaws associated with enzyme based glucose sensors such as complicated immobilization procedures, critical operating conditions, poor reproducibility and poor long-term stability [8], have steered researchers to explore non-enzymatic detection.

Over the past decades, tremendous efforts have been devoted in the development of reliable non-enzymatic glucose sensor which led to the utilization of metal, metal oxide and alloys, such as Pt, Au, Ag, Cu, Ni, Co, NiO, $NiCo_2O_4$, $NiCoO_2$, Co_3O_4 [9,10]. In spite of various catalytic materials available for glucose sensor, nickel (Ni) based nanomaterials [11,12] have captured more attention towards researchers, owing to wide linear range and excellent catalytic activity towards glucose oxidation in alkaline medium leading to $Ni(OH)_2$ and NiOOH species [13]. In spite of their high electrocatalytic activity, the surface fouling associated with glucose oxidation hinders its stability. Hence the need of a conductive nano structured substrate arises which can enhance the electrode stability and electron transfer toward oxidation of glucose of Ni.

Carbon based nanomaterials such as carbon nanotube (CNT) [14], graphene sheet (GS) [15], graphene nanoribbon (GNR) [16] and fullerene [17] with excellent physico-chemical properties can be considered as ideal supports for Ni catalyst nanoparticles. Graphene draws attention as an excellent catalyst support material due to its high specific surface area, good conductivity, electrochemical stability and low manufacturing cost. However the excellent properties of graphene are

* Corresponding author.
E-mail addresses: sivakumar.gomathi@gmail.com, gomathi@iist.ac.in (G. Nageswaran).

http://dx.doi.org/10.1016/j.materresbull.2017.10.020
Received 23 March 2017; Received in revised form 7 September 2017; Accepted 13 October 2017
Available online 28 October 2017
0025-5408/

suppressed by the restacking of the graphene layers due to π- π interactions. Recently a new trend in material science exploits in the synthesis of hybrid material, which can prevent restacking and enhance the surface area. There are several reports available on various hybrid materials for instance GS/CNT [18], GS/graphene oxide sheet (GOS) [19], GNR/CNT [20] and GS/GNR [21] and applied in various fields such as supercapacitor, solar cells and ultra-sensitive electrochemical sensors with relatively good performance.

To the best of our knowledge, no attempt has been made to promote the performance of non-enzymatic based glucose sensor through introduction of Ni nanoparticles with hybrid graphene of GS/GNR. In this work a synergistic combination of excellent properties of Ni, the catalytic material and hybrid graphene GS/GNR, the catalyst support, is aimed to enhance the electrocatalytic performance. We developed a novel highly sensitive non-enzymatic glucose sensor based on graphene sheet/graphene nanoribbon/nickel nanoparticles (GS/GNR/Ni), via in-situ chemical reduction method. The obtained hybrid material was characterized with different techniques and employed as non-enzymatic glucose sensor. The excellent performance of the sensor due to its electrocatalytic activity, stability, sensitivity and selectivity enables the determination of glucose in human serum.

2. Experimental

2.1. Reagents and apparatus

Graphite flakes (GF) with particle size < 20 μm, multi-walled carbon nanotube (MWCNT), carbon > 95% 6 − 9 nm O.D x 5 μm L, uric acid (UA) and dopamine (DA) were purchased from sigma Aldrich. 98% sulphuric acid (H_2SO_4), 88% ortho phosphoric acid (H_3PO_4), potassium permanganate ($KMnO_4$), 30% hydrogen peroxide (H_2O_2), 35% hydrochloric acid (HCl), hydrazine hydrate $(NH_2)_2{\cdot}H_2O$, nickel chloride ($NiCl_2{\cdot}6H_2O$), sodium hydroxide (NaOH), ethanol, poly vinyl pyrrolidine (PVP), dextrose, sucrose, sodium chloride (NaCl) and ascorbic acid (AA) were purchased from Merck India. All chemicals and reagents for electrochemical measurements were of analytical grade and used without further purification. All solutions were prepared with water from Millipore Autopure system (18.2 MΩ, Millipore Ltd., USA).

The microstructure of samples was observed by transmission electron microscopy (TEM) (FEI Quanta high resolution transmission electron microscope U.S.A.). X-ray diffraction (XRD) analysis was carried out to illustrate the structural and crystalline phase of the as-obtained samples (Xpert Pro, Philips, USA) using CuKα radiations (λ = 1.54˚A). Raman spectroscopy of the samples was carried out using a WiTech alpha 300 CRF system from Germany, excited with 532 nm.

2.1.1. Synthesis of graphene oxide sheets (GOS)

GOS was synthesized using improved method. Briefly, 9:1 ratio of concentrated H_2SO_4/H_3PO_4 was added to a mixture of GF and $KMnO_4$. The oxidation process was performed at 60 ˚C for 12 h with continuous stirring until a brown suspension is formed. This was further treated with 5 mL H_2O_2 (30%) to reduce the residual oxidants and intermediates to soluble sulphate. To remove the impurities such as chloride, sulphur etc., the suspension was centrifuged using distilled water, ethanol and acetone for several times. Then it was vacuum dried at 60 ˚C for 24 h.

2.1.2. Synthesis of graphene oxide ribbons (GOR)

GOR was synthesized by a novel strategy adopted by improved hummer's method. GOR was prepared by unzipping MWCNT by chemical oxidation. MWCNT was stirred with 98% sulphuric acid for 1 h at room temperature. After 1 h 88% ortho phosphoric acid is added to the mixture followed by potassium permanganate gradually. The reaction mixture was stirred for 4 h while keeping the temperature at 65 ˚C. Then 50 mL distilled water was added and stirred at room temperature for 30 min. The reaction was terminated by addition of water and 30% H_2O_2. The dispersion was washed by centrifugation and decantation. The final product was dried at 60 ˚C under vacuum for 12 h.

2.1.3. Synthesis of GS/GNR, Ni and GS/GNR/Ni

The synthesis routes of GS/GNR, Ni and GS/GNR/Ni are as described below.

GOS [22] and GOR [23] were taken in the ratio 10:1 and co-reduced with 15 mL $(NH_2)_2{\cdot}H_2O$ by stirring for 24 h at 40 ˚C. The product was washed with distilled water, ethanol and acetone. Further to increase the rate of deoxygenation, leading to better conductivity, the product was stirred with 15 mL HI for 24 h at 40 ˚C. The final product was washed with distilled water, ethanol and acetone and vacuum dried at room temperature for 24 h to obtain GS/GNR hybrid material [21].

Ni nanoparticles were synthesized by a chemical reduction method using $NiCl_2{\cdot}6H_2O$ as precursor. First 0.020 g of PVP was dissolved in a mixture of 15 mL ethanol and 60 mL water, followed by addition of 0.1 M NaOH solution and 0.05 M $NiCl_2.6H_2O$. After sonicating for 1 h, the mixture was reduced by 2 mL of $(NH_2)_2$. H_2O. Later washing with ethanol and distilled water for several times, the product was dried under vacuum at 60 ˚C for 12 h to obtain Ni nanoparticles.

GS/GNR/Ni was prepared by *in-situ* chemical reduction method as follows: GOS and GOR suspension (1.0 mg mL^{-1}) were mixed at the ratio of 1:1 and ultrasonically dispersed for 1 h in distilled water. Then 0.020 g of PVP was dissolved in 15 mL ethanol and 60 mL water at room temperature, followed by addition of 0.1 M NaOH solution and 0.05 M $NiCl_2{\cdot}6H_2O$. After sonicating for 1 h, the solution was reduced by 2 mL of $(NH_2)_2$. H_2O at 100 ˚C for 12 h. Later washing with ethanol and water for several times, the product was dried under vacuum at 60 ˚C for 12 h to obtain GS/GNR/Ni.

2.1.4. Fabrication of electrode and electrochemical measurement

The working electrode for non-enzymatic electrochemical sensing was fabricated as follows: Glassy carbon electrode (GCE) was polished with 0.3 mm and 0.05 mm gamma alumina particles, followed by rinsing and sonicating in distilled water and in ethanol, which was further dried under stream of nitrogen. GS/GNR, Ni and GS/GNR/Ni were dispersed in ethanol (1 mg/2 mL) by ultrasonication for more than 30 min. GCE was modified by coating with 7 μL suspension of GS/GNR/Ni by drop casting method on the electrode surface and dried at room temperature under vacuum for 12 h. For comparative evaluation, GCE electrode was coated with GS/GNR and Ni by the same procedure.

Electrochemical measurements were performed with a potentiostat/galvanostat PG 302N, AUT 83909 (Metrohm, Autolab, Netherlands) in conventional three-electrode system. A commercial GCE (3 mm diameter) was used as the working electrode. Pt wire and Ag/AgCl/saturated KCl were used as the counter and reference electrodes, respectively. All electrochemical experiments were performed at room temperature and all the potentials were reported against Ag/AgCl as reference electrode in 0.1 M NaOH electrolyte, which promote the dissociation of H_2O and gain high electrochemical signal compared with phosphate buffer saline.

The electrocatalytic performance of the modified electrodes using 0.1 M NaOH was investigated by cyclic voltammetry (CV) in potential range of 0 to 1 V. The effect of concentration of glucose was investigated by amperometric measurements performed in 0.1 M NaOH solution with the successive addition of different concentrations of glucose at an applied potential of + 0.5 V.

3. Results and discussion

Scheme 1 depicts the preparation of GS/GNR/Ni hybrid material via chemical reduction method and electrochemical oxidation of glucose. Firstly, Ni^{2+} were adsorbed onto the GOS and GOR surface through electrostatic interaction between Ni^{2+} and the functional groups (carboxyl, hydroxyl and epoxy groups) on GOS and GOR surface. Then, Ni $(OH)_2$ formed after the addition of NaOH precipitant in GOS and GOR

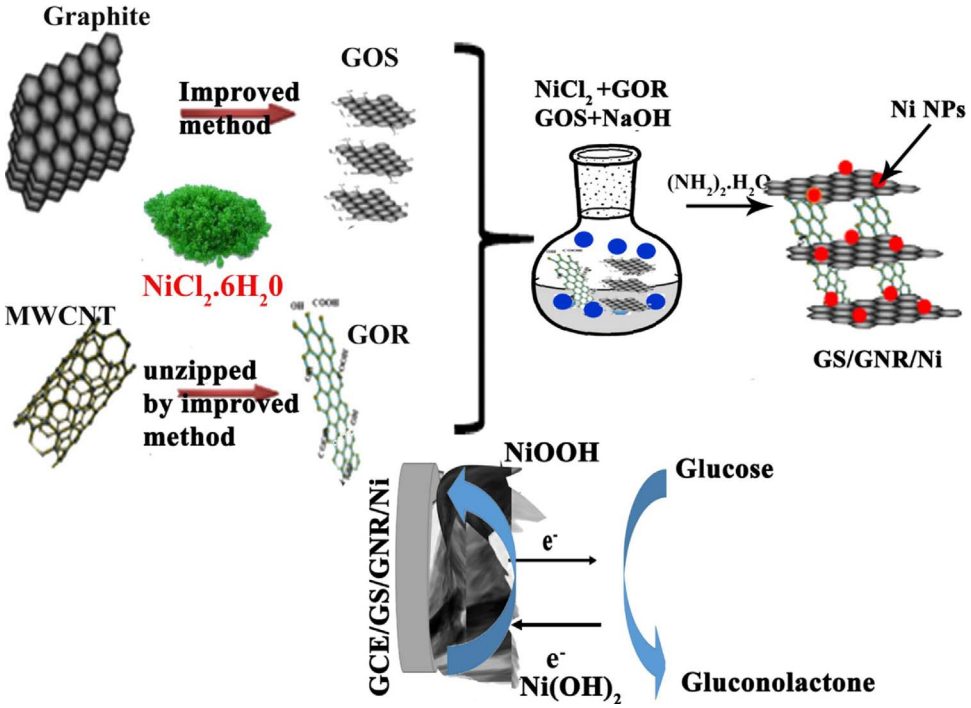

Scheme 1. Synthesis of GS/GNR/Ni and electrochemical glucose sensing.

network was co-reduced by hydrazine hydrate. During this process, the reducing agent plays its role in reduction of GOS and GOR, Ni^{2+} ions to Ni^0 nanoparticles, as well as in the growth of Ni nanoparticles into GS/GNR network.

XRD patterns of Ni, GS/GNR and GS/GNR/Ni are displayed in Fig. S1. The diffraction peak of Ni was found around 44.7°, 52° and 76.5° corresponding to the characteristic peaks of Ni (JCPDS card No. 04-0805), with an FCC lattice, which belong to (1 1 1), (2 0 0) and (2 2 0) planes, respectively. In the case of GS/GNR the diffraction peaks at 2θ = 25.2° and 44.4° corresponding to layered and hexagonal structured graphitic carbon indexed as (002) and (101) planes respectively [24,25]. The incorporation of Ni nanoparticles with GS/GNR in GS/GNR/Ni hybrid material was evidenced by the diffraction peaks at 2θ = 25.2°, 44.7°, 52° and 76.5°, corresponding to GS/GNR and Ni with an FCC lattice (1 1 1), (2 0 0) and (2 2 0) planes, respectively.

The Raman spectra of GS/GNR and GS/GNR/Ni hybrid materials were examined for further evidence of the successful incorporation of Ni on the GS/GNR and depicted in Fig. S2. The hybrid materials, exhibit two characteristic peaks at 1352 and 1581 cm^{-1} corresponding to D and G band respectively. D-band related to the occurrence of defects, due to the vibration of sp^3 bonded carbon atoms while G-band corresponding to sp^2 hybridised carbon is originated from the emission of Brillouin zone centered E_{2g} phonons [26]. The I_D/I_G ratio was effectively used to evaluate the degree of disorder in the sample; increase in the I_D/I_G ratio from 0.5 to 1.16 for the GS/GNR and GS/GNR/Ni was observed, which suggests that defects were introduced in the hybrid sample due to the destructive interaction of Ni with the GS/GNR, which can provide more active sites for the electrocatalytic oxidation of glucose [27].

The morphology of synthesized Ni nanoparticles and GS/GNR/Ni nanostructures was investigated by transmission electron microscopy and the obtained nanostructures are shown in Fig. 1.

The nanostructure of Ni nanoparticles exhibit dispersed sphere like morphology with an average size of 55 ± 2 nm as depicted in Fig. 1(a). Fig. 1(b) displaying the morphology of GS/GNR/Ni hybrid, describes the coexistence of Ni nanoparticles along with hybrid graphene. The morphology of hybrid graphene exhibits sheet like morphology with different transparencies indicating the difference in number of graphene layers corresponding to GS and small nanoribbon

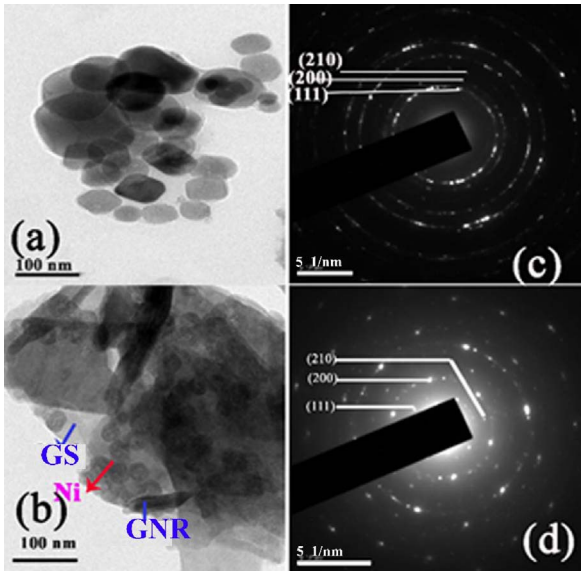

Fig. 1. TEM image of (a) Ni (b) GS/GNR/Ni (c) selected area energy diffraction (SAED) pattern of Ni and (d) GS/GNR/Ni.

like morphologies corresponding to GNR. Diffraction data obtained from SAED pattern of both Ni and GS/GNR/Ni are depicted in Fig. 1 (c and d). The lattice spacing of 0.24 nm and 0.21 nm which can be readily indexed to the (111) and (200) crystal planes respectively confirms the formation of crystalline structure of Ni nanoparticles. The bright spots in hexagonal pattern attributed to sp^2 −bonded carbon frameworks, along with diffraction spots at (111), (200) and (210) planes assigned to cubic Ni in GS/GNR/Ni hybrid are in good agreement with XRD results shown in Fig. S1.

In the case of GS/GNR the strong interaction between GS and GNR formed during the co- reduction of GOS and GOR helps in preventing the restacking of exfoliated graphene layers leading to the formation of hybrid network, resulting in increased surface area. Surface area of hybrid graphene (82.7 m^2/g) was increased nearly four times compared to reduced graphene oxide (20.7 m^2/g) as reported in our previous

work [21]. The incorporation of Ni nanoparticles with hybrid graphene led to the formation of complex network where the GNR and GS are intermeshed together with randomly interspersed Ni nanoparticles.

3.1. Electrochemical characterization

3.1.1. Electrocatalytic oxidation of glucose

The effect of concentration of the electrolyte (NaOH) on the electro activity of the catalytic material was investigated by CV measurements. The concentrations of NaOH used were 0.01, 0.1, 0.2, 0.3 and 0.4 M. The peak current increased with increasing NaOH concentration as shown in Fig. S3, which was attributed to the formation of more hydroxide ions in high concentration of NaOH. Chemisorbed hydroxide ions (OH-) facilitate a stronger interaction between glucose and Ni based electrode and decrease the activation energy for the oxidation of glucose as follows. First, OH- neutralises the protons generated during the dehydrogenation steps; second, the formation of glucose intermediate occurs at a faster rate in alkaline solution; and third, the conversion of glucose intermediate to gluconolactone with the formation of NiOOH catalyst, the concentration of which is influenced by OH-. Further increase in NaOH concentration results in decreased oxidation peak due to the blockage of active sites on the electrode by the increased concentration of hydroxide ions. Therefore, 0.1 M NaOH was selected as the optimal concentration for the further experiments.

The electrocatalytic behaviour of GCE, GS/GNR/GCE, Ni/GCE and GS/GNR/Ni/GCE were evaluated by CV in alkaline medium with and without addition of glucose and illustrated in Fig. 2. All CV experiments were carried out in the potential window of 0.0-1.0 V at a scan rate of 50 mV s^{-1}. The CV obtained at bare GCE and GS/GNR/GCE revealed no redox behaviour, indicating that both the electrodes do not undergo redox reaction in 0.1 M NaOH [28].

In contrast, owing to excellent electrocatalytic properties of Ni nanoparticles, Ni/GCE and GS/GNR/Ni/GCE modified electrodes exhibited a pair of well-defined redox peaks, under an alkaline solution with the anodic (E_{pa}) and cathodic (E_{pc}) peak potential of +0.5 V and +0.3 V vs. Ag/AgCl respectively, which correspond to the redox reaction that occurs between Ni nanoparticles and OH to form $Ni(OH)_2$/NiO(OH), indicating that the modified electrodes exhibited significant electro catalytic activity in the alkaline medium and the involved electrochemical reaction as follows:

$$Ni(OH)_2 + OH \rightarrow NiO(OH) + H_2O + e- \quad (1)$$

Moreover, the observed oxidation peak current of the GS/GNR/Ni/GCE (Fig. S4) was much higher than that of other electrodes. The superior electro catalytic performance of GS/GNR/Ni/GCE was attributed to the synergistic effect of GS/GNR hybrid network and Ni nanoparticles. In the hybrid network of GS/GNR/Ni, where Ni nanoparticles were uniformly dispersed on GS/GNR, the GS/GNR hybrid provides higher specific surface area, enhanced electrical conductivity and more active sites, providing a facile transport pathways for ions and offers unhindered diffusion of OH- during the electrochemical process. Ni nanoparticles serve as excellent catalytic active material for direct glucose oxidation, which would further enhance the electron transfer resulting to high sensitivity, lower detection limit and good selectivity towards glucose detection. Similar catalytic mechanism was exhibited in the Cu_2O nanocubes incorporated on GS structures [29].

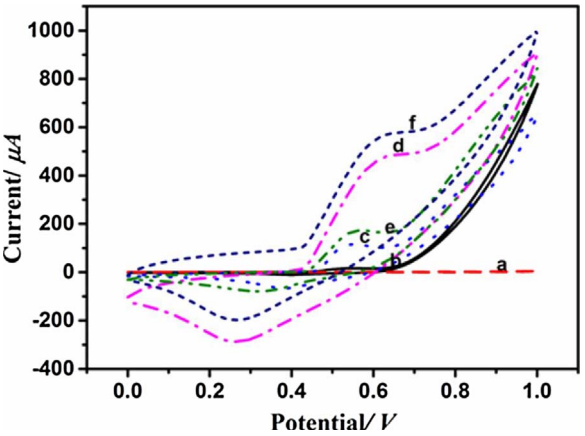

Fig. 2. CV response of bare GCE (a); GS/GNR/GCE (b); Ni/GCE (c) & (e); GS/GNR/Ni/GCE (d) & (f) in 0.1 M NaOH; (a, b, c, d − in absence of glucose, e, f − in presence of 0.1 mM glucose); scan rate: 50 mV s^{-1}.

Upon addition of glucose, the significant increase of the oxidation current was ascribed to the fact that Ni was oxidized to $Ni(OH)_2$ on the surface of the GS/GNR/Ni/GCE electrode (eqn (1)), and then glucose was catalytically oxidized to gluconolactone, further to gluconic acid by a hydrolyzation process (eqn (2 & 3)). In addition, due to the adsorption of glucose and the oxidized intermediates on the active sites in GS/GNR/Ni based electrode, the anodic peak potential shifts to a little positive direction. It was also ascribed to the diffusion limitation of glucose at the electrode surface; these results are consistent with the previous reported papers on Ni [30].

The mechanism for oxidation of glucose by Ni nanomaterials can be described by the following reactions [31,32].

$$NiO(OH) + glucose \rightarrow Ni(OH)_2 + gluconolactone \quad (2)$$

Finally, gluconolactone was turned into gluconic acid by hydrolysis:

$$Gluconolactone \rightarrow gluconic\ acid \quad (3)$$

The electro oxidation of glucose towards GS/GNR/Ni/GCE was investigated along with other electrodes such as Ni/GCE, GS/Ni/GCE, and GNR/Ni/GCE and illustrated in Fig. S5. Among the modified electrodes GS/GNR/Ni/GCE shows significant enhancement in oxidation peak currents. The excellent electrochemical performance observed at GS/GNR/Ni/GCE was ascribed to GS/GNR hybrid network which improves the glucose sensing not only by large surface area and better dispersion of Ni nanoparticles, and also by high electrical conductivity and charge transfer capability.

Moreover during co-reduction of GOS, GOR and $Ni(OH)_2$ the ample functional groups available in both the edges and basal of GOS and GOR, provides more anchoring sites for the incorporation of more Ni nanoparticles i.e catalytic site and enhance the rate of electron transfer between glucose and the electrode. Also the homogeneously dispersed Ni nanoparticles over the GS/GNR matrix extended the electroactive surface area of GS/GNR/Ni material, which further improved the adsorption of analyte.

3.1.2. Electro-kinetic studies

To evaluate the kinetics of glucose oxidation on the surface of GS/GNR/Ni/GCE, CVs were recorded at different scan rates ranging between 10 and 100 mV s^{-1} and depicted in Fig. S6. The peak potential for the oxidation of glucose shifts to positive values, along with increase in oxidation and reduction peak currents with increasing scan rate from 10 to 100 mV s^{-1} (Fig. S6 a and b). The linear relationship between the peak current and square root of scan rate with a linear regression equation of

$$I_p = 4.9608 + 1.40769^{\frac{1}{2}}\left(mV^{\frac{1}{2}}s^{-\frac{1}{2}}\right) R = 0.9972 \quad (4)$$

indicates that the oxidation of glucose on the surface of GS/GNR/Ni/GCE is diffusion controlled [33,34]. As shown in Fig. S6c, the E_{pa} was linearly dependent on the logarithm of the scan rate. The electrochemical parameters for instance electron-transfer coefficient (α) and apparent charge-transfer constant (k_s) can be calculated using Laviron's model [35].

$$E_{pa} = E^o + \frac{RT}{(1-\alpha)nF} ln\frac{1-\alpha}{m} \quad (5)$$

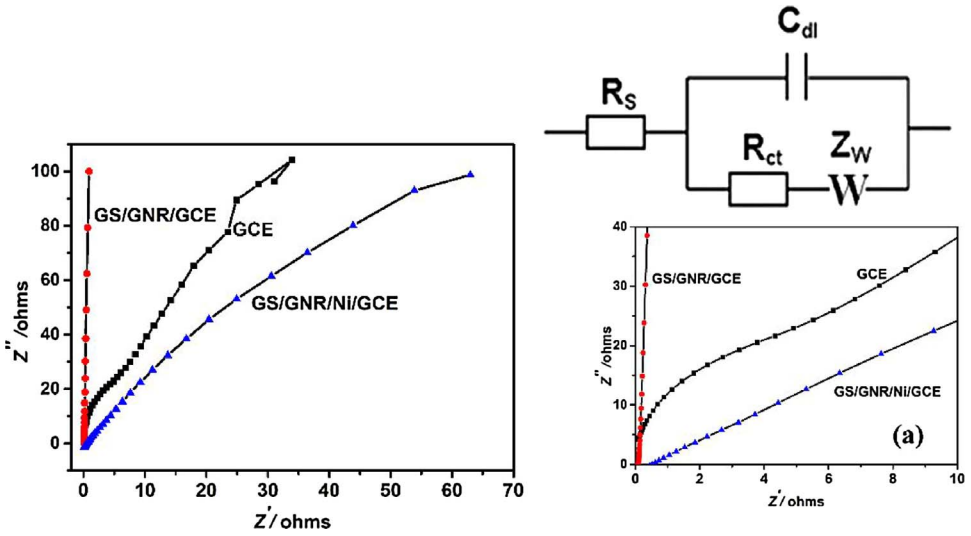

Fig. 3. Electrochemical impedance spectra of GCE, GS/GNR/GCE and GS/GNR/Ni/GCE electrodes in a 1 M KCl electrolyte with 5 mM $K_3[Fe(CN)_6]$ and 5 mM $K_4[Fe(CN)_6]$ with Randles circuit along with (a) magnified portion of Nyquist plot.

$$E_{pc} = E^0 - \frac{RT}{\alpha nF} ln\frac{\alpha}{m} \quad (6)$$

$$logK_s = \alpha \log(1-\alpha) + (1-\alpha)log\alpha - log\frac{RT}{nF\vartheta} - \frac{\alpha(1-\alpha)nF\Delta E_p}{2.3RT} \quad (7)$$

where m = (RT/F)(k_s/αn)–(8), n is the number of electrons transferred in the rate-determining step, ΔE_p is the peak potential separation, R is the gas constant (8.314 J mol^{-1} K^{-1}), T is the room temperature (298 K) and F is Faraday's constant (96,485C mol^{-1}), and ϑ is the scan rate. α and k_s as determined from these plots and Eq. (7) are 0.43 and 2.37 s^{-1}, respectively was higher than Nafion/SBA-15-Cu (II) modified GCE [44]. This indicates that the GS/GNR/Ni/GCE electrode can effectively promote electron transfer.

3.1.3. Impedance studies of modified electrodes

Electrochemical impedance spectroscopy (EIS), a powerful method to investigate the interfacial process between the electrode and electrolyte.

The impedance measurements of GCE, GS/GNR/GCE and GS/GNR/Ni/GCE were performed in 1 M KCl with 5 mM $K_3[Fe(CN)_6]$ and 5 mM $K_4[Fe(CN)_6]$ and shown in Fig. 3. The obtained experimental data of the three electrode were fitted by a Randles equivalence circuit model, including the Warburg impedance (Z_w), the charge transfer resistance (R_{ct}), the double layer capacitance (C_{dl}), and ohmic resistance of the electrolyte (R_s). The EIS includes a semicircle portion and a line. The semicircle portion at higher frequency expresses the electron-transfer limited process, and the corresponding diameter is equal to the charge-transfer resistance (R_{ct}). The line at lower frequency characters the diffusion process. After fitting the data, among the three modified electrodes, the R_{ct} value of GS/GNR/Ni/GCE is found to be significantly less (17 Ω) compared to GS/GNR/GCE (140 Ω), and GCE (15700 Ω). The decreased charge transfer resistance was attributed to the hybrid network of graphene sheet and graphene nanoribbon which not only enhances the surface area available for Ni incorporation but also accelerates the rate of electron transfer, thereby increasing the electrical conductivity and decreasing the charge transfer resistance, effectively enhancing the detecting sensitivity and shortening of the response time.

3.1.4. Optimization of potential in glucose sensing

The effect of increase in concentration of glucose towards GS/GNR/Ni/GCE was studied elaborately by amperometric method. Considering that the amperometric response of the sensor can strongly be influenced by the applied potential, we have investigated the optimum potential for the amperometric determination of glucose. The amperometric response of GS/GNR/Ni/GCE electrode with successive addition of 0.1 mM of glucose in 0.1 M NaOH in the potential range of +0.4 to +0.7 V vs. Ag/AgCl was illustrated in Fig. S7. When the applied potential is increased from +0.4 V to +0.5 V, the oxidation current of glucose was increased gradually with the successive addition of 0.1 mM glucose. As shown in the inset, the response current reaches the maximum value at +0.5 V.

However, the current response was decreased when the applied potential further increases. The reason for this phenomenon can be explained by the fact that the generation of many interfering substances interacted with the electrode, which leads to the decayed current. By comparison, the applied potential of +0.5 V enabled the best performance, which was selected as the suitable working potential for glucose detection in subsequent experiments, which is also potentially beneficial for elimination of interferences from electroactive substances such as DA, UA and AA.

3.1.5. Amperometric detection of glucose

The sensitivity of GS/GNR/Ni/GCE towards glucose detection was investigated by adding different concentrations of glucose into the electrolyte. Amperometric responses of GS/GNR/Ni/GCE upon successive addition of certain amount of glucose to 0.1 M NaOH was carried out under constant magnetic stirring at the optimum potential of 0.5 V. Fig. 4A illustrates the current response recorded with respect to time for the GS/GNR/Ni/GCE with the incremental addition of glucose and Fig. 4B represents calibration curve (current vs concentration) for the electrochemical responses of the GS/GNR/Ni/GCE with the successive injection of 10 μL glucose with concentration ranging between 5 nM and 5 mM. The wide linear range might be due to the larger surface area with more electro active sites for the oxidation of glucose at GS/GNR/Ni/GCE. We observed a step-like increase of responding current towards glucose and it attained 95% of the steady current within 5 s demonstrating its fast response. In addition, the fast response may be due to the promoted electron transfer and excellent catalytic activity provided by Ni nanoparticles and the hybrid structure of GS/GNR [36].

Meanwhile, from the slope of the calibration curve, the sensitivity of the GS/GNR/Ni/GCE was found to be 2.32 mA/ mM cm^{-2} for a concentration range of 5 nM to 5 mM with a correlation coefficient of R^2 = 0.9975. The limit of detection (LOD) is determined using equation (9).

$$LOD = \frac{3*\alpha}{slopeofthecalibrationcurve} \quad (9)$$

where σ is the standard deviation of the blank. From the calculation, the LOD of the sensor was found to be 2.5 nM with a signal-to-noise ratio of 3.

The above electrochemical measurements show GS/GNR/Ni/GCE

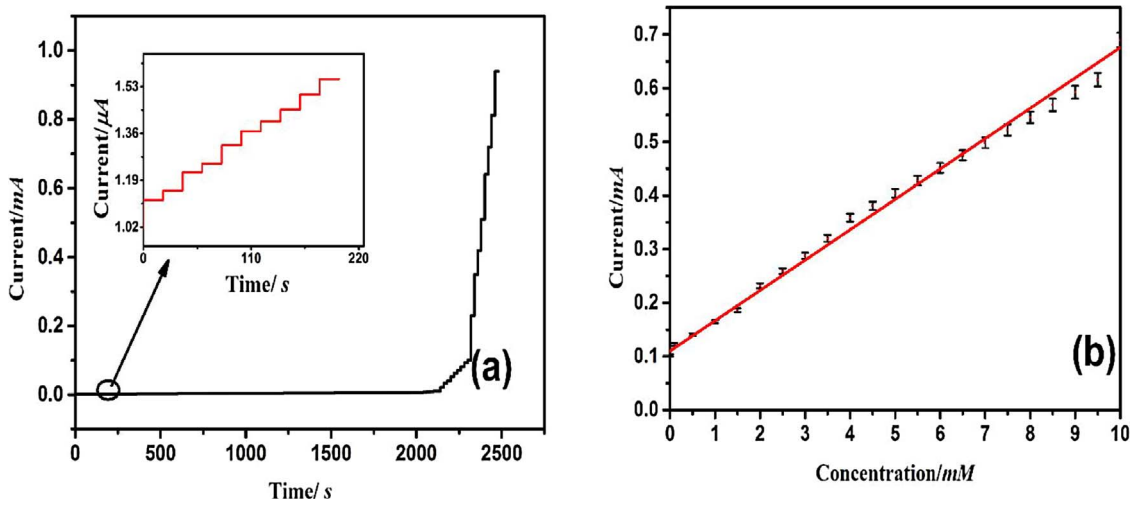

Fig. 4. (a) Amperometric i-t response of GS/GNR/Ni/GCE with the successive addition of different concentrations of glucose in the range of 5 nM − 5 mM in 0.1 M NaOH at an applied potential of 0.5 V vs. Ag/AgCl with time interval 20 s (Inset: Magnified view of time response from 0 − 220 s) and (b) Calibration curve for glucose concentration ranging between 5 nM − 5 mM with the error bars indicating the standard deviation of triplicate determinations.

exhibited higher catalytic activity for glucose oxidation with higher sensitivity and lower detection limit, which can be attributed to the excellent electro catalytic property toward the oxidation of glucose owing to the unique structure of hybridised graphene sheet and nanoribbon which provides enhanced area for loading more Ni nanoparticles which provide many active sites for the oxidation of glucose. And also facilitate the diffusion of glucose molecules and accelerate the electron transfer.

A list of the reported non-enzymatic glucose sensors based on Ni is shown in Table 1; it can be seen that the analytical performance of the sensor proposed in this study is better than most of the previous studies in terms of sensitivity, LOD, and linear range.

Table 1
Comparison of performance of as-fabricated glucose sensor with other glucose sensors reported previously.

Electrode	Sensitivity	Linear range	Detection limit	References
GS/GNR/Ni	2.32 mA mM^{-1} cm^{-2}	5 nM–5 mM	2.5 nM	This work
PVP[a]/GS/NiNPs[c]-CS[b]	103.8 μA mM^{-1} cm^{-2}	0.1 μM-0.5 mM	30 nM	[37]
CNT/Ni NAs[d]	1381 μA mM^{-1} cm^{-2}	0.5–10 mM	1 μM	[25]
Ni NWs[e]	367 μA mM^{-1} cm^{-2}	1 μM–5 mM	1 μM	[38]
CNT/Ni	1384.1 μA mM^{-1} cm^{-2}	5 μM–2 mM	2 μM	[39]
PAA[f]/Ni	–	5 μM–12 mM	0.65 μM	[40]
NiNPs/GN[g]	865 μA mM^{-1} cm^{-2}	5 μM–0.55 mM	1.85 μM	[41]
NiNPs/CNF[h]	420.4 μA mM^{-1} cm^{-2}	2 μM–2.5 mM	1 μM	[42]
NiNPs/BDD[i]	1040 μA mM^{-1} cm^{-2}	10 μM–10 mM	2.7 μM	[43]
Ni/PSi[j]-CPE[k]	–	2 μM–5000 μM	0.2 μM	[45]
RGO/$Ni(OH)_2$[l]/GCE	11.43 mA mM^{-1} cm^{-2}	2 μM–3.1 mM	0.6 μM	[46]
NiO[m]/HMS[n]/GCE	2.39 mA mM^{-1} cm^{-2}	1.67 μM–6.87 mM	0.53 μM	[47]
AgNPs[o]/CPE	540.7 μA mM^{-1}	28.6 μM–9.80 mM	5.5 μM	[48]
s-NiO[p]/GD[q]	36.13 mA mM^{-1} mm^{-2}	Upto 10.0 mM	0.9 μM	[49]
AgNPs/F-MWCNTs[r]/GCE	1057.3 mA mM^{-1}	1.3–1000 mM	0.03 mM	[50]
$Ni(OH)_2$/NND[s]	3.20 and 1.41 mA mM^{-1} cm^{-2}	0.02–1 mM and 1–9 mM	1.2 μM	[51]
Pd[t]/NiO/Nile–rGO/CPE	–	0.020–20.0 mM	2.2 μM	[52]

[a] PVP- poly vinyl pyrrolidene.
[b] CS − chitoson.
[c] NPs − nanoparticles.
[d] NAs- nanostructuted arrays.
[e] NWs − nanowires.
[f] PAA − poly(azure A).
[g] GN − Graphene sheet.
[h] NiNPs-CNF- Ni nanoparticles loaded carbon nanofiber.
[i] BDD- boron-doped diamond.
[j] Psi-porous silicon.
[k] CPE − carbon paste electrode.
[l] $Ni(OH)_2$- nickel hydroxide.
[m] NiO-nickel oxide.
[n] HMS-hollow micro sphere.
[o] Ag-Silver.
[p] s-NiO- porous NiO nanosheets.
[q] GD-graphite disks.
[r] F-MWCNTs-functionalized multiwall carbon nanotubes.
[s] NND-nitrogen-incorporated nanodiamonds.
[t] Pd-palladium.

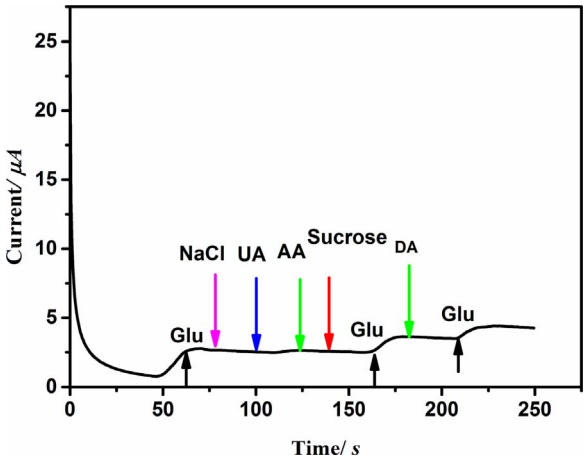

Fig. 5. Effect of interferents, 0.01 mM of AA, UA, NaCl, sucrose and DA on the response of the GS/GNR/Ni/GCE to glucose of 0.5 mM in NaOH at 0.5 V.

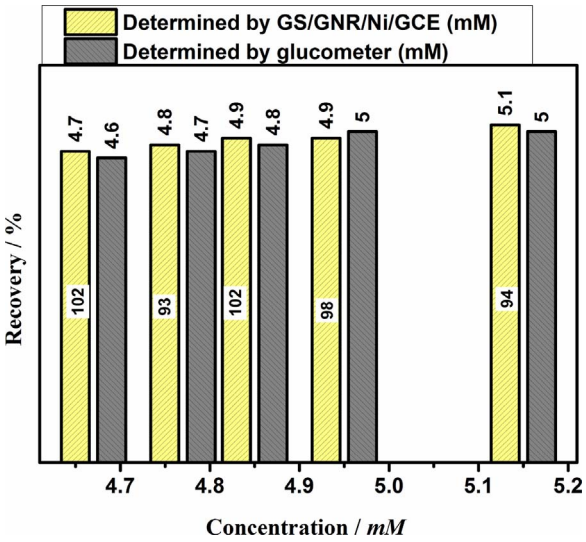

Fig. 6. The bar chart showing the glucose recovery in human serum samples as determined between commercial glucose meter and GS/GNR/Ni/GCE.

3.1.6. Interference, stability and reproducibility of the sensor

In physiological fluids, endogenous species such as ascorbic acid (AA), uric acid (UA), sodium chloride (NaCl), sucrose and dopamine (DA) generally co-exist with glucose. Hence, the effect of these species towards the selectivity of GS/GNR/Ni/GCE on glucose detection was investigated and illustrated in Fig. 5. While, the normal physiological level of glucose in human blood is 4.4–6.6 mM and various endogenous species which could hinder the performance of GS/GNR/Ni/GCE are below 0.1 mM. The interference experiment study was undertaken with the addition of 0.5 mM glucose, followed by consecutive injection of 0.01 mM of each ascorbic acid (AA), uric acid (UA), dopamine (DA), NaCl and sucrose by amperometric method. Negligible current response observed towards addition of interferents demonstrates that the glucose sensor based on GS/GNR/Ni/GCE has high selectivity for possible practical applications.

Moreover, long-term stability of the fabricated GS/GNR/Ni/GCE electrode was investigated by measuring the change in current response over 30 days period. And the obtained results are depicted in Fig. S8. The electrode was stored in air at room temperature and their current response was investigated every three days after injecting 0.5 mM glucose to 0.1 M NaOH electrolyte. The response current was decreased by only 8.7% from its original current and became saturated after 30 days, which suggests that the fabricated GS/GNR/Ni/GCE has good long term stability. Furthermore, the stability of sensor was also evaluated by measuring the response current of 30 successive CV measurements of 0.5 mM glucose in 0.1 M NaOH with single electrode. No obvious change in peak current was observed as shown in Fig. S9 which reveals that Ni nanoparticles incorporated with GS/GNR efficiently enhance the stability of the sensor material towards consecutive cycle.

The reproducibility of as-fabricated GS/GNR/Ni/GCE electrode was also verified using the amperometric responses of glucose (500.0 μmol L^{-1}) at a series of freshly prepared five electrodes. The relative standard deviation (R.S.D.) of 2.16%, indicates that the fabricated sensor possesses good reproducibility.

3.1.7. Real sample analysis

The reliability of the GS/GNR/Ni/GCE sensor was also evaluated by determining the glucose level in human serum using standard addition method. In brief, five serum samples obtained from healthy donors were diluted with 10 mL of 0.1 M NaOH. The obtained results were consistent with the blood glucose meter (Fig. 6) with recovery rates of glucose detection of ≥95%. This strongly suggest that the fabricated GS/GNR/Ni/GCE electrode can be successfully utilized for glucose detection in blood samples without any pre-treatment step.

This superior performance of GS/GNR/Ni based non-enzymatic glucose sensor can be ascribed to the excellent conductivity of GS/GNR, where the GNR incorporated between the GS layers could prevent the restacking of graphene sheets, thereby increases the electron transfer from electrode to electrolyte and *vice versa*. Furthermore, the incorporated GNR with GS effectively increase the surface area of GS/GNR, provides more sites for Ni nanoparticles, where glucose can adsorb and quicken the rate of oxidation.

4. Conclusions

A simple, facile and effective chemical reduction method has been exploited to incorporate Ni nanoparticles over the graphene hybrid consisting of graphene sheet and graphene nanoribbon. The hybrid of GS and GNR could significantly reduce the aggregation and stacking between graphene, which resulted in enhanced surface area and wide porous structure of the GS/GNR hybrids. Due to these excellent properties, the hybrid material of Ni nanoparticles incorporated in GS/GNR showed remarkably improved electrocatalytic response of glucose and exhibited excellent performances for the amperometric determination of glucose with rapid response, low detection limit, high sensitivity and selectivity, wide linear range and good long-term stability for the oxidation of glucose. Finally, the fabricated sensor was used for the determination of glucose in human blood serum.

Acknowledgements

Authors thank IIST, VRC VSSC, Trivandrum and PSG Coimbatore for XRD, Raman spectroscopy and TEM.

References

[1] S. Wild, G. Roglic, A. Green, R. Sicree, H. King, Global prevalence of diabetes: estimates for theyear 2000 and projections for 2030, Diabetes Care 27 (2004) 1047–1053, http://dx.doi.org/10.2337/diacare.27.5.1047.
[2] S. Song, L. Sun, L. Yuan, T. Sun, Y. Zhao, W. Zuo, et al., Method to determine enantiomeric excess of glucose by nonchiral high-performance liquid chromatography using circular dichroism detection, J. Chromatogr. A 1179 (2008) 125–130, http://dx.doi.org/10.1016/j.chroma.2007.11.092.
[3] W. Kanchana, T. Sakai, N. Teshima, S. Katoh, K. Grudpan, Successive determination of urinary protein and glucose using spectrophotometric sequential injection method, Anal. Chim. Acta. 604 (2007) 139–146, http://dx.doi.org/10.1016/j.aca.2007.10.010.
[4] H. Kang, Y. Lee, K.J. Lee, B. Jung, Optical polarimetry probe system for glucose concentration monitoring, SPIE (2008) 686307–686309, http://dx.doi.org/10.1117/12.764293.
[5] X. Liu, W. Niu, H. Li, S. Han, L. Hu, G. Xu, Glucose biosensor based on gold nanoparticle-catalyzed luminol electrochemiluminescence on a three-dimensional sol–gel network, Electrochem. Commun. 10 (2008) 1250–1253, http://dx.doi.org/

10.1016/j.elecom.2008.06.009.
[6] J. Singh, P. Khanra, T. Kuila, M. Srivastava, A.K. Das, N.H. Kim, et al., Preparation of sulfonated poly(ether?ether?ketone) functionalized ternary graphene/AuNPs/chitosan nanocomposite for efficient glucose biosensor, Process Biochem. 48 (2013) 1724–1735, http://dx.doi.org/10.1016/j.procbio.2013.07.025.
[7] L.C. Clark, C. Lyons, Electrode systems for continuous monitoring In cardiovascular surgery, Ann. N. Y. Acad. Sci. 102 (1962) 29–45, http://dx.doi.org/10.1111/j.1749–6632.1962. tb13623.x.
[8] R. Wilson, A.P.F. Turner, Glucose oxidase: an ideal enzyme, Biosens. Bioelectron. 7 (1992) 165–185, http://dx.doi.org/10.1016/0956-5663(92)87013-F.
[9] G. Wang, X. He, L. Wang, A. Gu, Y. Huang, B. Fang, et al., Non-enzymatic electrochemical sensing of glucose, Microchim. Acta. 180 (2013) 161–186, http://dx.doi.org/10.1007/s00604-012-0923-1.
[10] P. Si, Y. Huang, T. Wang, J. Ma, Nanomaterials for electrochemical non-enzymatic glucose biosensors, RSC Adv. 3 (2013) 3487–3502, http://dx.doi.org/10.1039/C2RA22360K.
[11] X. Xiao, J.R. Michael, T. Beechem, A. McDonald, M. Rodriguez, M.T. Brumbach, et al., Three dimensional nickel-graphene core-shell electrodes, J. Mater. Chem. 22 (2012) 23749–23754, http://dx.doi.org/10.1039/C2JM35506J.
[12] J. Wang, W. Bao, L. Zhang, A nonenzymatic glucose sensing platform based on Ni nanowire modified electrode, Anal. Methods 4 (2012) 4009, http://dx.doi.org/10.1039/c2ay25759a.
[13] M. Fleischmann, K. Korinek, D. Pletcher, The oxidation of organic compounds at a nickel anode in alkaline solution, J. Electroanal. Chem. Interfacial Electrochem. 31 (1971) 39–49, http://dx.doi.org/10.1016/S0022-0728(71)80040-2.
[14] S. Iijima, C. Brabec, A. Maiti, J. Bernholc, Structural flexibility of carbon nanotubes, J. Chem. Phys. 104 (1996) 2089–2092, http://dx.doi.org/10.1063/1.470966.
[15] A.K. Geim, K.S. Novoselov, The rise of graphene, Nat. Mater. 6 (2007) 183–191, http://dx.doi.org/10.1038/nmat1849.
[16] D.V. Kosynkin, A.L. Higginbotham, A. Sinitskii, J.R. Lomeda, A. Dimiev, B.K. Price, et al., Longitudinal unzipping of carbon nanotubes to form graphene nanoribbons, Nature 458 (2009) 872–876, http://dx.doi.org/10.1038/nature07872.
[17] B.C. Yadav, R. Kumar, Structure, properties and applications of fullerene, Int. J. Nanotechnol. Appl. 2 (2016) 15–24.
[18] X. Dong, Y. Ma, G. Zhu, Y. Huang, J. Wang, M.B. Chan-Park, et al., Synthesis of graphene?carbon nanotube hybrid foam and its use as a novel three-dimensional electrode for electrochemical sensing, J. Mater. Chem. 22 (2012) 17044, http://dx.doi.org/10.1039/c2jm33286h.
[19] V. Mani, S.M. Chen, B.S. Lou, Three dimensional graphene oxide-carbon nanotubes and graphene-carbon nanotubes hybrids, Int. J. Electrochem. Sci. 8 (2013) 11641–11660.
[20] M. Liu, Y.-E. Miao, C. Zhang, W.W. Tjiu, Z. Yang, H. Peng, et al., Hierarchical composites of polyaniline-graphene nanoribbons-carbon nanotubes as electrode materials in all-solid-state supercapacitors, Nanoscale 5 (2013) 7312–7320, http://dx.doi.org/10.1039/c3nr01442h.
[21] J. Lavanya, N. Gomathi, High-sensitivity ascorbic acid sensor using graphene sheet/graphene nanoribbon hybrid material as an enhanced electrochemical sensing platform, Talanta 144 (2015) 655–661, http://dx.doi.org/10.1016/j.talanta.2015.07.018.
[22] D.C. Marcano, D.V. Kosynkin, J.M. Berlin, A. Sinitskii, Z. Sun, A. Slesarev, et al., Improved synthesis of graphene oxide, ACS Nano 4 (2010) 4806–4814, http://dx.doi.org/10.1021/nn1006368.
[23] A.L. Higginbotham, D.V. Kosynkin, A. Sinitskii, Z. Sun, J.M. Tour, Lower-Defect graphene oxide nanoribbons from multiwalled carbon nanotubes, ACS Nano 4 (2010) 2059–2069, http://dx.doi.org/10.1021/nn100118m.
[24] W. Zhang, X. Zhang, L. Zhang, G. Chen, Fabrication of carbon nanotube-nickel nanoparticle hybrid paste electrodes for electrochemical sensing of carbohydrates, Sens. Actuators B Chem. 192 (2014) 459–466, http://dx.doi.org/10.1016/j.snb.2013.11.016.
[25] J. Zhu, J. Jiang, J. Liu, R. Ding, Y. Li, H. Ding, et al., CNT-network modified Ni nanostructured arrays for high performance non-enzymatic glucose sensors, RSC Adv. 1 (2011) 1020, http://dx.doi.org/10.1039/c1ra00280e.
[26] L.M. Malard, M.A. Pimenta, G. Dresselhaus, M.S. Dresselhaus, Raman spectroscopy in graphene, Phys. Rep. 473 (2009) 51–87, http://dx.doi.org/10.1016/j.physrep.2009.02.003.
[27] G. Li, H. Huo, C. Xu, Ni 0.31 Co 0.69 S 2 nanoparticles uniformly anchored on a porous reduced graphene oxide framework for a high-performance non-enzymatic glucose sensor, J. Mater. Chem. A 3 (2015) 4922–4930, http://dx.doi.org/10.1039/C4TA06553K.
[28] X. Gao, Y. Lu, M. Liu, S. He, W. Chen, Sub-nanometer sized $Cu_6(GSH)_3$ clusters: one-step synthesis and electrochemical detection of glucose, J. Mater. Chem. C 3 (2015) 4050–4056, http://dx.doi.org/10.1039/C5TC00246J.
[29] M. Liu, R. Liu, W. Chen, Biosensors and Bioelectronics Graphene wrapped Cu_2O nanocubes: non-enzymatic electrochemical sensors for the detection of glucose and hydrogen peroxide with enhanced stability, Biosens. Bioelectron. 45 (2013) 206–212, http://dx.doi.org/10.1016/j.bios.2013.02.010.
[30] P. Sivasakthi, G.N.K. Ramesh Bapu, M. Chandrasekaran, Pulse electrodeposited nickel-indium tin oxide nanocomposite as an electrocatalyst for non-enzymatic glucose sensing, Mater. Sci. Eng. C 58 (2016) 782–789, http://dx.doi.org/10.1016/j.msec.2015.09.036.
[31] J. Wang, G. Chen, M.P. Chatrathi, Nickel amperometric detector prepared by electroless deposition for microchip electrophoretic measurement of alcohols and sugars, Electroanalysis 16 (2004) 1603–1608, http://dx.doi.org/10.1002/elan.200302996.
[32] L.-M. Lu, L. Zhang, F.-L. Qu, H.-X. Lu, X.-B. Zhang, Z.-S. Wu, et al., A nano-Ni based ultrasensitive nonenzymatic electrochemical sensor for glucose: enhancing sensitivity through a nanowire array strategy, Biosens. Bioelectron. 25 (2009) 218–223, http://dx.doi.org/10.1016/j.bios.2009.06.041.
[33] Z. Shen, W. Gao, P. Li, X. Wang, Q. Zheng, H. Wu, et al., Highly sensitive nonenzymatic glucose sensor based on nickel nanoparticle-attapulgite-reduced graphene oxide-modified glassy carbon electrode, Talanta 159 (2016) 194–199, http://dx.doi.org/10.1016/j.talanta.2016.06.016.
[34] E. Laviron, General expression of the linear potential sweep voltammogram in the case of diffusionless electrochemical systems, J. Electroanal. Chem. Interfacial Electrochem. 101 (1979) 19–28, http://dx.doi.org/10.1016/S0022-0728(79)80075-3.
[35] Z. Liu, Y. Guo, C. Dong, A high performance nonenzymatic electrochemical glucose sensor based on polyvinylpyrrolidone–graphene nanosheets–nickel nanoparticles?chitosan nanocomposite, Talanta 137 (2015) 87–93, http://dx.doi.org/10.1016/j.talanta.2015.01.037.
[36] R. Zhang, S. He, C. Zhang, W. Chen, Three-dimensional Fe- and N-incorporated carbon structures as peroxidase mimics for fluorescence detection of hydrogen peroxide and glucose, J. Mater. Chem. B 3 (2015) 4146–4154.
[37] J. Wang, W. Bao, L. Zhang, A nonenzymatic glucose sensing platform based on Ni nanowire modified electrode, Anal. Methods 4 (2012) 4009–4013, http://dx.doi.org/10.1039/C2AY25759A.
[38] T. Choi, S.H. Kim, C.W. Lee, H. Kim, S.-K. Choi, S.-H. Kim, et al., Synthesis of carbon nanotube–nickel nanocomposites using atomic layer deposition for high-performance non-enzymatic glucose sensing, Biosens. Bioelectron. 63 (2015) 325–330, http://dx.doi.org/10.1016/j.bios.2014.07.059.
[39] T. Liu, Y. Luo, J. Zhu, L. Kong, W. Wang, L. Tan, Non-enzymatic detection of glucose using poly(azure A)-nickel modified glassy carbon electrode, Talanta 156–157 (2016) 134–140, http://dx.doi.org/10.1016/j.talanta.2016.04.053.
[40] B. Wang, S. Li, J. Liu, M. Yu, Preparation of nickel nanoparticle/graphene composites for non-enzymatic electrochemical glucose biosensor applications, Mater. Res. Bull. 49 (2014) 521–524, http://dx.doi.org/10.1016/j.materresbull.2013.08.066.
[41] A. Zhong, X. Luo, L. Chen, S. Wei, Y. Liang, X. Li, Enzyme-free sensing of glucose on a copper electrode modified with nickel nanoparticles and multiwalled carbon nanotubes, Microchim. Acta. 182 (2015) 1197–1204, http://dx.doi.org/10.1007/s00604-014-1443-y.
[42] Y. Liu, H. Teng, H. Hou, T. You, Nonenzymatic glucose sensor based on renewable electrospun Ni nanoparticle-loaded carbon nanofiber paste electrode, Biosens. Bioelectron. 24 (2009) 3329–3334, http://dx.doi.org/10.1016/j.bios.2009.04.032.
[43] K.E. Toghill, L. Xiao, M.A. Phillips, R.G. Compton, The non-enzymatic determination of glucose using an electrolytically fabricated nickel microparticle modified boron-doped diamond electrode or nickel foil electrode, Sens. Actuators B Chem. 147 (2010) 642–652, http://dx.doi.org/10.1016/j.snb.2010.03.091.
[44] M. Shamsipur, Z. Karimi, M. Amouzadeh Tabrizi, S. Rostamnia, Highly sensitive non-enzymatic electrochemical glucose sensor by Nafion/SBA-15-Cu (II) modified glassy carbon electrode, J. Electroanal. Chem. 799 (2017) 406–412, http://dx.doi.org/10.1016/j.jelechem.2017.06.029.
[45] A.A. Ensafi, N. Ahmadi, B. Rezaei, Nickel nanoparticles supported on porous silicon flour, application as a non-enzymatic electrochemical glucose sensor, Sens. Actuators B Chem. 239 (2017) 807–815, http://dx.doi.org/10.1016/j.snb.2016.08.088.
[46] Y. Zhang, F. Xu, Y. Sun, Y. Shi, Z. Wen, Z. Li, Assembly of Ni(OH)2 nanoplates on reduced graphene oxide: a two dimensional nanocomposite for enzyme-free glucose sensing, J. Mater. Chem. 21 (2011) 16949, http://dx.doi.org/10.1039/c1jm11641j.
[47] S. Ci, T. Huang, Z. Wen, S. Cui, S. Mao, D.A. Steeber, et al., Nickel oxide hollow microsphere for non-enzyme glucose detection, Biosens. Bioelectron. 54 (2014) 251–257, http://dx.doi.org/10.1016/j.bios.2013.11.006.
[48] M. Ghiaci, M. Tghizadeh, A.A. Ensafi, N. Zandi-Atashbar, B. Rezaei, Silver nanoparticles decorated anchored type ligands as new electrochemical sensors for glucose detection, J. Taiwan Inst. Chem. Eng. 0 (2015) 1–7, http://dx.doi.org/10.1016/j.jtice.2016.03.013.
[49] H. Liu, X. Wu, B. Yang, Z. Li, L. Lei, X. Zhang, Three-Dimensional porous NiO nanosheets vertically grown on graphite disks for enhanced performance non-enzymatic glucose sensor, Electrochim. Acta 174 (2015) 745–752, http://dx.doi.org/10.1016/j.electacta.2015.06.062.
[50] A.A. Ensafi, N. Zandi-Atashbar, B. Rezaei, M. Ghiaci, M.E. Chermahini, P. Moshiri, Non-enzymatic glucose electrochemical sensor based on silver nanoparticle decorated organic functionalized multiwall carbon nanotubes, RSC Adv. 6 (2016) 60926–60932, http://dx.doi.org/10.1039/C6RA10698F.
[51] C.-Y. Ko, J.-H. Huang, S. Raina, W.P. Kang, A high performance non-enzymatic glucose sensor based on nickel hydroxide modified nitrogen-incorporated nanodiamonds, Analyst 138 (2013) 3201–3208, http://dx.doi.org/10.1039/c3an36679k.
[52] A.A. Ensafi, Z. Ahmadi, M. Jafari-Asl, B. Rezaei, Graphene nanosheets functionalized with Nile blue as a stable support for the oxidation of glucose and reduction of oxygen based on redox replacement of Pd-nanoparticles via nickel oxide, J. Electroanal. Chem. 173 (2015) 619–629, http://dx.doi.org/10.1016/j.electacta.2015.05.109.